Applied Physics A (2020) 126:484
https://doi.org/10.1007/s00339-020-03670-8

Applied Physics A
Materials Science & Processing

An insight into the low doping efficiency of Al in sol–gel-derived ZnO:Al films: role of the dopant chemical state

M. W. Zhu[1] · H. B. Ma[1] · P. H. Jin[2] · Y. N. Jin[1] · N. Jia[2] · H. Chen[1] · C. Z. Liu[1]

Received: 9 March 2020 / Accepted: 26 May 2020 / Published online: 4 June 2020
© Springer-Verlag GmbH Germany, part of Springer Nature 2020

Abstract

We prepared aluminum-doped zinc oxide (ZnO:Al, AZO) films by a sol–gel method and investigated the effect of doping on the electrical properties of AZO films in the Al doping concentration range of 0.5–3.0 at.%. The negative effect of Al dopants on the carrier mobility counteracted their positive effect on the carrier concentration and the resistivity of the films remained almost constant at the optimum Al doping level of 0.5 at.%. Moreover, the doping efficiency of Al dopant decreased with increasing doping level and the maximum efficiency was not higher than 50% even at the optimum doping concentration. The microstructure and chemical composition of the films were examined by X-ray diffraction, scanning electron microscopy and X-ray photoelectron spectroscopy to elucidate the mechanism behind the low doping efficiency of Al dopant in the sol–gel-derived AZO films. The reason was attributed to the passivation of the dopant in two forms, defect complex $n\mathrm{Al}_{\mathrm{Zn}}$–$V_{\mathrm{Zn}}$ originating from the dopant–defect reaction in the ZnO grains and aluminum oxide phase segregating at the ZnO grain boundaries.

Keywords Transparent conductive oxide · Sol–gel process · Aluminum doping · Doping efficiency · Chemical state

1 Introduction

Zinc oxide (ZnO), a wide-bandgap semiconductor (E_g = 3.4 eV), has the common properties of transparent conductive oxides (TCO) along with the possible coexistence of high conductivity and excellent transparency. Moreover, ZnO has advantages including nontoxicity, high stability in hydrogen plasma, and high abundance. The conductivity of ZnO can be increased using extrinsic dopants such as group III elements (B, Al, Ga, In) of the periodic table. In particular, Al-doped ZnO (AZO) is emerging as a promising substitute for tin-doped indium oxide (ITO) [1]. Recently, AZO has been extensively investigated for use in various applications such as solar cells, architectural glass coatings, and other optoelectronic devices [2–4].

The preparation method of an AZO film affects its resistivity, which is restricted by the highest carrier concentration and mobility achieved in AZO films. AZO films with high conductivity and excellent transparency can be obtained using physical vapor deposition (PVD) [5, 6]. However, the industrial production of films by PVD is limited because of the complex and expensive vacuum equipment required. Highly conductive AZO films using solution method have always been pursued and the advantage comes to the fore when preparing large-area and homogeneous films [7, 8]. The sol–gel method has thus attracted much interest even though the resistivity of sol–gel-derived AZO films is usually 1–2 orders of magnitude higher than that of AZO films deposited by PVD, as shown in Table 1. Both the optimum doping level of Al and the carrier concentration of AZO films in sol–gel method are much lower than those in PVD methods. These factors are closely related to the solubility of Al dopant and its low doping efficiency; i.e., not all the dopants are introduced into the ZnO lattice and, therefore, efficiently donate free electrons. The crystallization and growth of films produced by the sol–gel method are only activated by thermal energy, which is typically of the

✉ C. Z. Liu
czliu@sau.edu.cn

[1] School of Materials Science and Engineering, Shenyang Aerospace University, Shenyang 110136, People's Republic of China

[2] Key Laboratory for Anisotropy and Texture of Materials (Ministry of Education), School of Material Science and Engineering, Northeastern University, Shenyang 110819, People's Republic of China

Table 1 Electrical properties of Al-doped ZnO thin films prepared by different methods

Optimum doping content	Method[a]	Carrier concentration (cm^{-3})	Resistivity (Ω cm)	Hall mobility ($cm^{-2} V^{-1} s^{-1}$)	References
3.0 at% Al	RFMS	5.52×10^{20}	9.13×10^{-4}	12.4	[50]
4.6 at.% Al	RFMS	1.02×10^{21}	2.72×10^{-4}	22.5	[5]
4.6 at.% Al	DCMS	4.9×10^{20}	4.07×10^{-4}	31.3	[51]
4.2 at.% Al	PLD	1.54×10^{21}	8.54×10^{-5}	47.5	[52]
4.6 at.% Al	PLD	1.50×10^{21}	1.43×10^{-4}	29.1	[6]
4.6 at.% Al	MOCVD	5.2×10^{20}	6.22×10^{-4}	19.3	[53]
3.0 at.% Al	ALD	7.74×10^{19}	5.6×10^{-3}	14.4	[54]
1.18 at.% Al	SP	5.63×10^{20}	8.62×10^{-4}	12.8	[55]
0.5 at.% Al	CBD	1.2×10^{20}	5×10^{-3}	10.9	[7]
2.0 at.% Al	Sol–gel	1.02×10^{20}	3.59×10^{-3}	17.1	[34]
1.4 at.% Al	Sol–gel	1.21×10^{20}	8.19×10^{-3}	6.3	[22]
1.0 at.% Al	Sol–gel	5.2×10^{19}	7.12×10^{-3}	16.8	[56]
0.5 at.% Al	Sol–gel	8.73×10^{19}	4.42×10^{-3}	16.2	Our work

[a] *RFMS* radio frequency magnetron sputtering, *PLD* pulsed laser deposition, *MOCVD* metal organic chemical vapor deposition, *ALD* atomic layer deposition, *SP* spray pyrolysis, *CBD* chemical bath deposition

order of 0.1 eV and much lower than that of plasma-assisted methods like magnetron sputtering (MS) and pulsed laser deposition (PLD) (> 1 eV) [9]. This limits the diffusivity and chemical reactivity of the dopant and, therefore, inherently lowers the solubility. Then improvement in doping efficiency is critical for decreasing the resistivity of sol–gel-derived AZO films.

Much work has focused on the effect of doping level on the resistivity of sol–gel-derived AZO films [10–12]. However, the mechanism behind the low doping efficiency of Al is not well understood. In this work, ZnO films with different levels of Al doping are prepared by the sol–gel method. The Al doping level is chosen to lie in the range of 0–3.0 at.% to obtain ZnO films with fully soluble and partly soluble Al. In combination with the microstructure and the chemical composition of the AZO films, the effect of Al doping level on the electrical properties of the films is systematically investigated. The solubility and chemical state of Al dopant are analyzed to explore the reason behind the low doping efficiency of sol–gel-derived AZO films.

2 Experimental procedure

Zinc acetate [$Zn(CH_3COO)_2$•$2H_2O$] was first dissolved in a solution of 2-methoxyethanol ($CH_3OC_2H_4OH$) and monoethanolamine (MEA, $HOC_2H_4NH_2$) at room temperature. The concentration of zinc acetate was 0.75 mol L^{-1} and the molar ratio of MEA to zinc acetate was kept at 1.0. The mixture became clear and homogeneous after stirring at 70 °C for 30 min. To realize Al doping, aluminum chloride ($AlCl_3.6H_2O$) was added to the zinc solution as a dopant source after the above procedure. The Al concentration, defined as 100 × [Al]/[Al + Zn], was strictly kept at 0, 0.5, 1.5, and 3.0 at.%. Transparent light yellow solutions with different Al content were obtained after stirring for another 30 min. These solutions served as the coating precursor after aging for more than 24 h at room temperature. Standard float glass (Schott glass) was used as a substrate and was cleaned before use in an ultrasonic bath for 15 min sequentially with acetone, ethanol, and distilled water. The above solutions were dip-coated on the glass substrates to obtain initial films. The initial films were dried at 80 °C for 20 min in air and then heated at 480 °C for 30 min after each coating procedure. The coating procedure was repeated five times altogether for all the samples discussed in the present work. After the coating procedure was complete, the samples were annealed under vacuum (base pressure ~ 10^{-3} Pa) at 400 °C for 60 min.

Transmittance spectra were obtained using an ultraviolet–visible spectrophotometer (Hitachi, U-3400). The resistivity and Hall coefficient of the films were measured at room temperature by the van der Pauw method (Ecopia HMS-3000). X-ray diffraction (XRD) patterns of the AZO films were determined by a Rigaku RINT2000 X-ray diffractometer using copper *Kα* radiation. The surface morphologies of the films were characterized by a field-emission scanning electron microscope (SEM, Ultra Plus). The valence states of different elements in the films were detected by X-ray photoelectron spectroscopy (XPS, RIBER LAS-3000) using monochromatic Al *Kα* radiation with a photon energy of 1486.6 eV. To measure the fresh surface without contamination from air, the films were etched in a vacuum chamber by Ar^+ for 50 s before XPS detection. Binding energies were calibrated to the C1s binding energy of 284.6 eV.

3 Results and discussion

3.1 Opto-electrical properties of AZO films with different Al doping levels

Figure 1a shows the transmittance spectra of AZO films with different Al doping concentrations. The average optical transmission of the films in the visible range (400–800 nm) was as high as 85%. The introduction of Al dopant decreased the transmittance of the AZO films, especially at short wavelength, but the Al doping content had little effect on the optical transmission of the films. The absorption edge of the films shifted to shorter wavelength (blue shift) with increasing Al doping concentration. The apparent bandgap (E_g) of the films was calculated according to the following equation [13] using Tauc plots:

$$\alpha h\nu = C(h\nu - E_g)^{1/2}, \quad (1)$$

where C is a constant, α is the absorption coefficient, and $h\nu$ is the photon energy. According to the optical spectra, E_g of the AZO films increased with rising Al doping concentration, i.e., $E_{3.0} \approx E_{1.5} > E_{0.5} > E_0$. Based on Burstein–Moss effect, E_g of ZnO is theoretically closely related to the carrier concentration of the films irrespective of the many-body effect [14, 15]. Thus, the increase of E_g indicated an increase of the carrier concentration in the AZO films with rising Al doping content.

Figure 1b confirms the increasing tendency of the carrier concentration in the AZO films with Al doping concentration. Conduction electrons in ZnO films mainly originate from the intrinsic donors, such as oxygen vacancies (V_O) and zinc interstitials (Zn_i). The doping of trivalent Al^{3+} in the lattice (Al_{Zn}) donates extra electrons for the conduction process in AZO films. The sharp increase in carrier concentration upon the incorporation of 0.5 at.% Al indicated a larger equilibrium concentration of Al_{Zn} than that of intrinsic defects in this AZO film. However, the carrier concentration increased nonlinearly with the Al doping level. The carrier concentration of the films increased slowly and remained almost constant above an Al doping content of 1.5 at.%. Therefore, excess Al dopant (> 1.5 at.%) makes little contribution to the improvement of the conductivity of AZO films. Conversely, the carrier mobility always decreased upon the introduction of Al dopant ions because of the increased number of carrier scattering centers, consistent with other work [16]. The decrease in carrier mobility was possibly attributed to the corresponding increase in grain boundary scattering and ionized impurity scattering, depending on the microstructure and carrier concentration [17, 18]. The film resistivity first decreased sharply and then increased slowly with rising Al doping level. The negative effect of Al dopant ions on carrier mobility counteracted their positive effect on carrier concentration and the resistivity of the films remained almost constant when the optimum Al doping level was reached. The minimum resistivity of 4.41×10^{-3} Ω cm was obtained for the AZO film with an Al doping content of 0.5 at.%, as shown in Fig. 1b.

From the above results, the carrier concentration in AZO film was much higher than that in pure ZnO film. Therefore, we assume that all electrons come from the doped Al in the films and every activated Al ion supplies one electron. Therefore, the carrier concentration represents the concentration of the activated doped Al per cubic centimeter. Thus, the doping efficiency was calculated according to the equation $n \times 100/4.14 \times 10^{20} C_{Al}$, where n is the carrier concentration and C_{Al} is the doping level. As shown in Fig. 2, the Al doping efficiency decreased with increasing doping level, i.e., higher doping efficiency was achieved at lower Al doping concentration. It has been concluded from the bulk form of ZnO that the equilibrium solution of Al in ZnO films should be lower than 3 at.% and the substituted atoms Al_{Zn} are mostly expected to form below the solubility limit in the films [19–21]. However, the doping efficiency was no higher than 50% even for the film with 0.5 at.% Al, which was thought to totally dissolve in ZnO, indicating that not every soluble Al ion can donate electrons. Figure 2 also presents some data from Ref. [22–37] for comparison with the doping efficiency of our films. The same tendency was observed. Additionally, the experimental data were scattered over a wide range at low doping level, suggesting the change

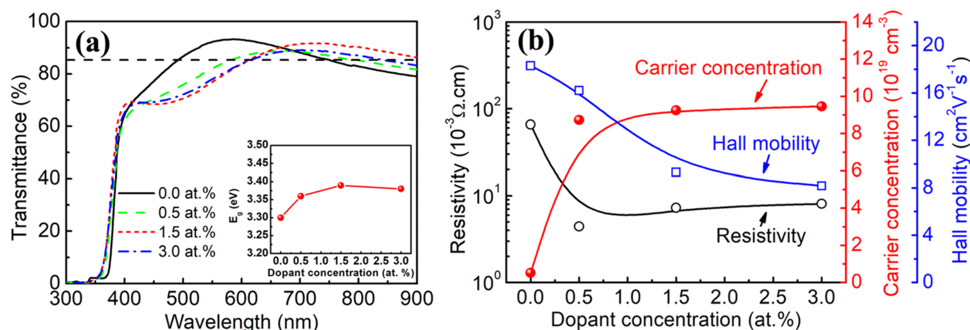

Fig. 1 **a** Optical transmittance and **b** electrical properties of the Al-doped ZnO thin films with different dopant concentrations

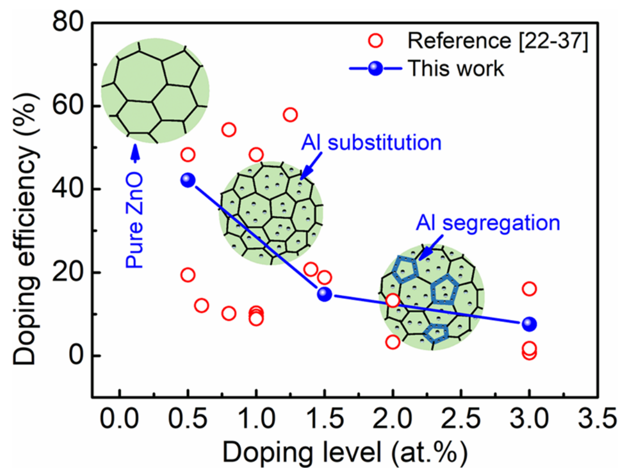

Fig. 2 Doping efficiency of the sol–gel-derived AZO films

in the position of the dopant under different growth conditions. Therefore, the low doping efficiency of Al dopant was necessarily related to the variation in the solubility and the chemical state of the dopant.

3.2 Stress and microstructure evolution of AZO films

Figure 3 shows the XRD patterns of AZO films with different Al doping concentrations. Peaks from three main planes appeared in the XRD pattern for the pure ZnO film (JCPDS no. 36-1451) and the intensity of the (002) peak increased with Al content, indicating the strengthening *c*-axis preferential orientation in the AZO films. The shoulder peaks in Fig. 3b come from the diffraction of Kα_2 ray, which is especially obvious for pure ZnO (with an intensity ratio of about 2:1 of the two peaks). Furthermore, the (002) peak shifted to higher angle with increasing Al doping concentration, indicating that the lattice parameters and, therefore, the residual stress of the films changed, as shown in Table 2. The in-plane stress (σ) of the films was calculated using Eq. (2) based on the biaxial strain model [38].

$$\sigma = \frac{2C_{13}^2 - C_{33}(C_{11} + C_{12})}{C_{13}} \times \frac{(c - c_0)}{c_0}, \quad (2)$$

where $C_{11} = 209.7$ GPa, $C_{12} = 121.1$ GPa, $C_{13} = 105.1$ GPa, and $C_{33} = 210.9$ GPa are the elastic stiffness constants of bulk ZnO, and c and c_0 are the lattice constants of ZnO films and the corresponding bulk value, respectively. The calculated results are shown in Fig. 3c and Table 2. The negative values obtained for σ indicated the compressive stress in the films. It was found that σ first decreased with increasing Al doping concentration below 1.5 at.% and then

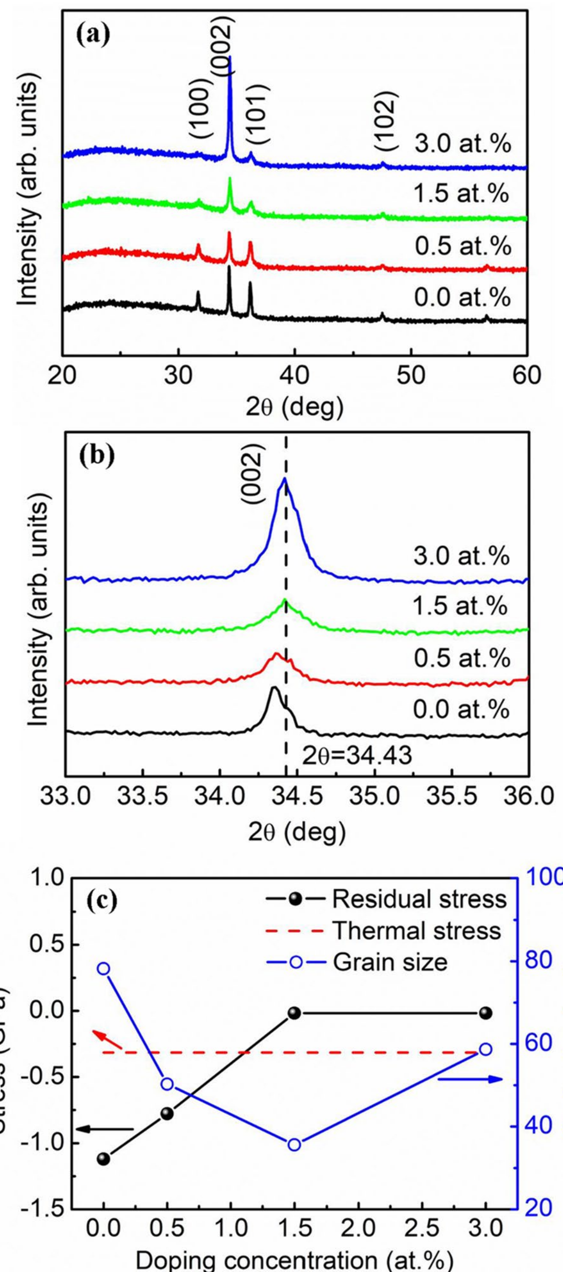

Fig. 3 **a** XRD patterns of AZO thin films with different Al doping levels. **b** Corresponding enlarged view of the XRD patterns. **c** Residual stress and grain size of AZO films with different Al doping levels. The dashed line shows the thermal stress under the assumption that the coefficients α_s and α_f are constant at different temperatures

remained almost constant up to an Al doping concentration of 3.0 at.%, i.e., σ was closely related to the doping level of Al in the AZO films.

Figure 3c also shows the change in grain size with the doping level. The variation tendency in grain size suggested that the grain growth process had a minor effect on the change in σ. The intrinsic stress depending on the defect concentration was thought to dominate over extrinsic stress

Table 2 Structural parameters of the AZO thin films (c_{bulk} = 5.205 Å)

Doping content	2 theta (°)	c (Å)	ε (%)	σ (GPa)	FWHM (°)	D (nm)
0.0 at.% Al	34.34	5.218	0.192	− 1.12	0.101	78.2
0.5 at.% Al	34.37	5.214	0.173	− 0.778	0.164	50.3
1.5 at.% Al	34.42	5.207	0.038	− 0.0017	0.225	35.6
3.0 at.% Al	34.42	5.207	0.038	− 0.0017	0.140	58.7

in the AZO films. The compressive stress in pure ZnO films has been attributed to the formation of Zn_i and V_O [39]. The substitution of Zn by Al was favorable for the release of compressive stress in the ZnO films. Therefore, the decrease of residual stress in the ZnO films with increasing Al doping concentration up to 1.5 at.% suggested the effective doping of Al below 1.5 at.%. This tendency confirmed the change in the carrier concentration. Further increasing the Al doping content had little effect on the residual stress in the films, indicating that Al dopant ions no longer substituted Zn in the ZnO lattice. Then the solubility of Al in ZnO films should be smaller than 1.5 at.%, consistent with the results from Ref. [8]. The excess Al dopant was thought to segregate as aluminum oxide phase at the grain boundary of ZnO. The possible existing state of Al is schematically shown in Fig. 2.

The surface and cross-sectional images of AZO films is shown in Fig. 4. Dense films of about 150 nm are obtained in the present work. Position of Al in the films strongly affected the growth mode of ZnO films and their microstructures. Different growth modes were observed with the

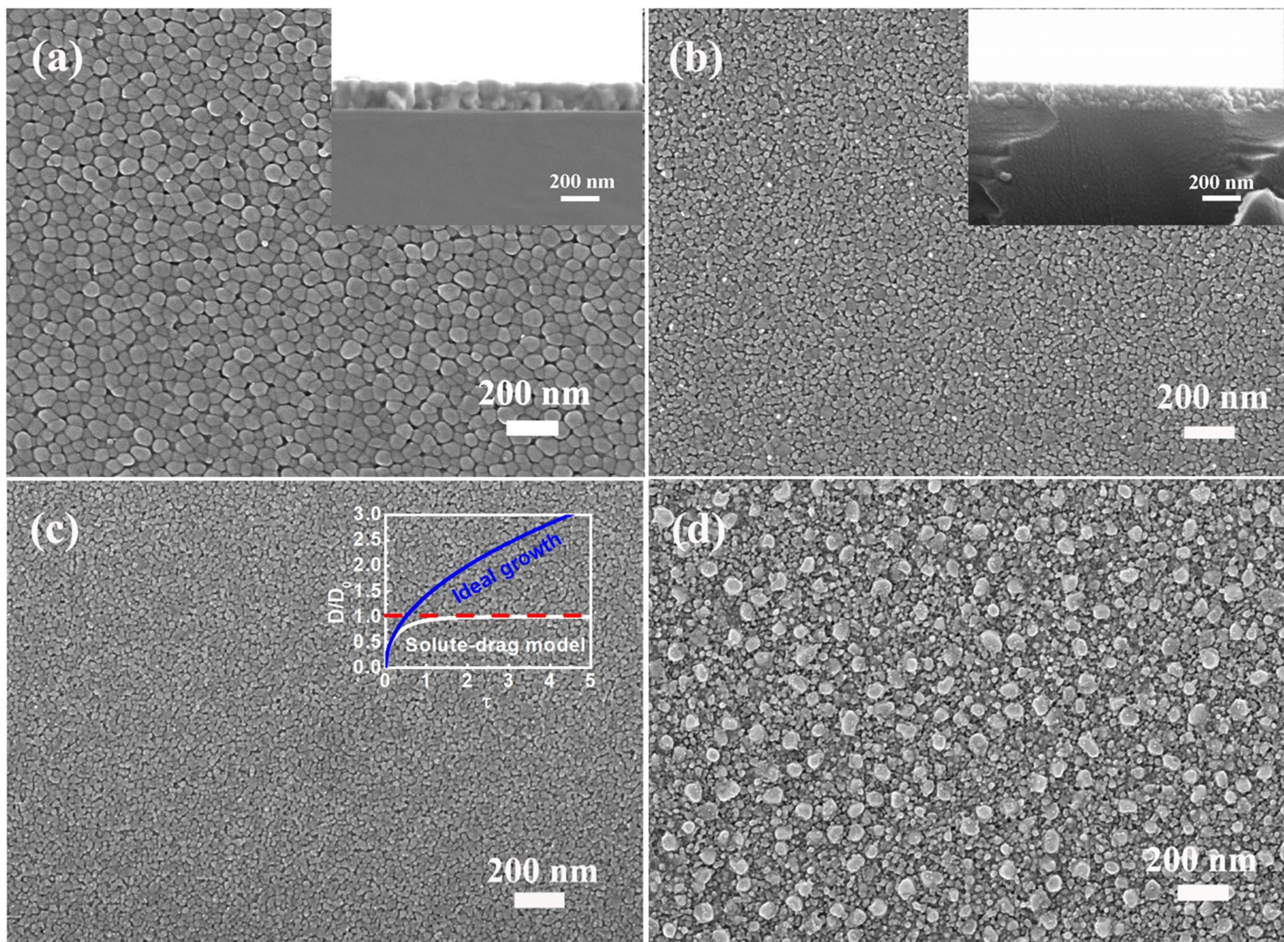

Fig. 4 Surface morphologies of AZO films with different Al dopant contents, **a** 0, **b** 0.5 at.%, **c** 1.5 at.%, **d** 3.0 at.%. The insets in **a** and **b** show the corresponding cross-sectional images of AZO films. The inset in **c** shows the simulated result by the solute drag model, where D_0 is the maximum grain size that ZnO can attain after doping and D is the grain size of ZnO at different growth time t (τ is a variable proportional to t), respectively

variation of Al doping level, as shown in Fig. 4. The pure ZnO film consisted of homogeneous grains with an average size of ~ 80 nm, indicating a normal grain growth process. The grain size sharply decreased first with the introduction of Al dopant, consistent with the results of Ohyama et al. [10]. The stagnation effect of Al dopant on the ZnO grain growth process was well simulated using the solute drag model proposed in Ref. [40], as shown in the inset of Fig. 4c. The pure ZnO grew following the ideal growth mode while the introduction of Al suppressed the growth of ZnO. This resulted in the significant grain refinement and the grain size saturates with the further increased growth time. The refinement in grain size necessarily induced more segregation of Al dopant ions. However, further increase of the Al dopant content to 3.0 at.% led to an inhomogeneous distribution of grain size and some anomalously large grains appeared on the film surface. This abnormal grain growth was possibly caused by the segregation of aluminum oxide at the grain boundaries of ZnO. The critical dopant concentration of 1.5 at.% for the change in growth mode was consistent with the above results.

Therefore, the low doping efficiency above the concentration of 1.5 at.% could be mainly ascribed to the insoluble Al dopant. However, this was not responsible for the low doping efficiency at lower doping level where the dopant was thought to dissolve in the film. Damm et al. [11] also found that the tetrahedral occupation of Al (Al_{Zn}) in ZnO films changed with the doping level and the mere increase of substitutional Al was not sufficient to render the film more conductive. This suggested the unwanted formation of some defect complex in the films. The Al_{Zn} donors could be passivated by the defect complexes [41, 42]. Meanwhile, the solubility of Al under equilibrium conditions was thought to be lower than 1.5 at.% in the present work, setting a doping electron limit of 6.4×10^{20} cm^{-3}. However, the maximum carrier concentration in our films was 9.46×10^{19} cm^{-3}, which is far below this limit. The difference between the experimental and theoretical carrier concentrations further confirmed the considerable effect of such complexes on the electrical properties of the AZO films.

3.3 XPS analysis of AZO films with different Al doping levels

The presence of defects or defect complexes can be reflected by the changes in the chemical state of species in such films. Figure 5 shows the chemical state of oxygen in the films. A slight shift of binding energy was observed and the shape of O 1 s peak became more asymmetric with increasing Al doping level. The O 1 s peaks were resolved into different peaks; detailed fittings are presented in Fig. 2b–d. The loosely bound oxygen on the original surface of the AZO films was eliminated by Ar^+ etching. The high-energy peak at 531.3 eV was associated with the adsorbed oxygen at the grain boundary (O_{II}), while the low-energy peak at 530.1 eV corresponded to the lattice oxygen (O_I) in the ZnO films

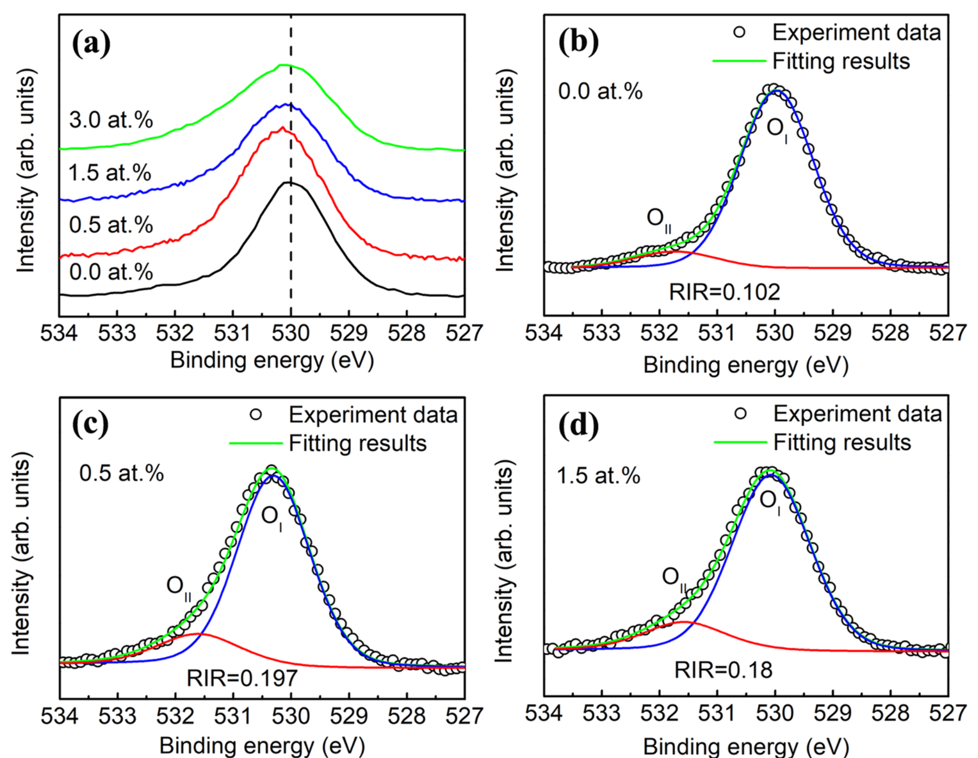

Fig. 5 **a** O 1*s* spectra of AZO films with different Al doping concentrations and **b**–**d** corresponding fitting results

[43]. The relative intensity ratio (RIR = O_{II}/O_{I}) of the two oxygen species indicated the variation in the concentration of the adsorbed oxygen in the films, which was thought as a trapping tank for the electrons. The RIR values slightly increased upon doping but remained almost constant with increasing Al doping level. The existence of adsorbed oxygen partly explained the low doping efficiency of Al dopant but could not account for the variation in doping efficiency.

Figure 6a shows the chemical state of Al in AZO films with different Al doping concentrations. The binding energy of Al metal is 72.9 eV and that of aluminum oxide is at 74.6 eV [44]. The binding energy of Al in the 0.5 at.% Al-doped ZnO film was at 73.5 eV, suggesting that Al exists in a state different from its metallic or fully oxidized state. Theoretical calculations and experimental results showed that the doped Al energetically preferred to substitute Zn sites to form a donor Al_{Zn} instead of an interstitial Al (Al_i) [45]. Thus, the peak at 73.5 eV was attributed to the formation of Al_{Zn}. However, the binding energy of the Al peak did not remain constant; it continuously increased with Al concentration, reaching 74.0 eV for the film with an Al concentration of 3.0 at.%. The increase in binding energy indicated that the chemical state of Al in the films shifted to a more oxidized state, corresponding to the formation of a secondary phase, like Al_2O_3 or $ZnAl_2O_4$.

Figure 6b presents the chemical state of Zn in the AZO films with different Al contents. The binding energy of the Zn $2p_{3/2}$ peak was located between 1021 and 1022 eV and the energy gap between Zn $2p_{1/2}$ and Zn $2p_{3/2}$ was 23 eV. This confirmed that the oxidized state of Zn was dominant in all the films. For the undoped ZnO film, the binding energy was lower than the reference line at 1020.8 eV and self-doped Zn_i was thought to act as a shallow intrinsic donor in ZnO [46, 47]. The binding energy of Zn increased to 1022 eV upon the introduction of 0.5 at.% Al; Al_{Zn} prevailed in this film. The positive shift of the peak positions of AZO films with increasing Al concentration has also been found for other AZO systems [48, 49]. This indicates that the solid-soluble Al in the ZnO lattice affected the chemical environment of Zn in the films and the number of Zn_i decreased simultaneously. Conversely, further increasing the Al doping level to 1.5 at.% lowered the binding energy of Zn, although it was still larger than that of the undoped ZnO film. The anomalous change in Zn valence state with increasing Al doping level suggested the occurrence of different dopant–defect reactions and $n\mathrm{Al}_{Zn}$–V_{Zn} was proposed as the main resultant defect complex. According to the defect chemistry in Eqs. (3) and (4), the formation of the $n\mathrm{Al}_{Zn}$–V_{Zn} complex increased the concentration of Zn_i under the current equilibrium conditions, which accounted for the shift in the binding energy of Zn spectra with increasing Al doping observed in Fig. 5b.

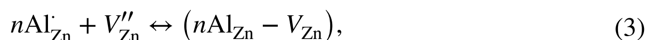

$$n\mathrm{Al}_{Zn}^{\cdot} + V_{Zn}'' \leftrightarrow \left(n\mathrm{Al}_{Zn} - V_{Zn}\right), \tag{3}$$

$$\mathrm{Zn}_{Zn} \leftrightarrow \mathrm{Zn}_{i}^{\cdot\cdot} + V_{Zn}''. \tag{4}$$

This trend stopped in the films with Al concentrations above 1.5 at.%, where the Zn state remained stable even when the Al doping level was raised to 3.0 at.%. According to the above analysis, segregation of Al_2O_3 or $ZnAl_2O_4$ occurred at the ZnO grain boundaries, which had little effect on the chemical state of Zn. Therefore, the Al doped in the films readily became a neutralized impurity in two forms: compensation of Al_{Zn} by intrinsic defects originating from the dopant–defect reaction in the ZnO grains and segregation as an oxide phase at the ZnO grain boundaries. Accordingly, the chemical state of Al in the AZO films strongly depended on its doping level: Al_{Zn} dominated in the Al doping range below 0.5 at.%, $n\mathrm{Al}_{Zn}$–V_{Zn} prevailed when the concentration of Al_{Zn} increased between 0.5 at.% and 1.5 at.%, whereas aluminum oxide existed in the films with an Al doping level above 1.5 at.%.

Consequently, the high resistivity and low doping efficiency of the AZO films produced by the sol–gel method is attributed to the following reasons. First, the crystallization and growth of AZO under equilibrium conditions limited the solubility of Al in ZnO. This resulted in low solubility (≤ 1.5 at%) of Al in the films. Excess Al existed as aluminum oxide segregated at the ZnO grain boundaries, setting the possible upper limit

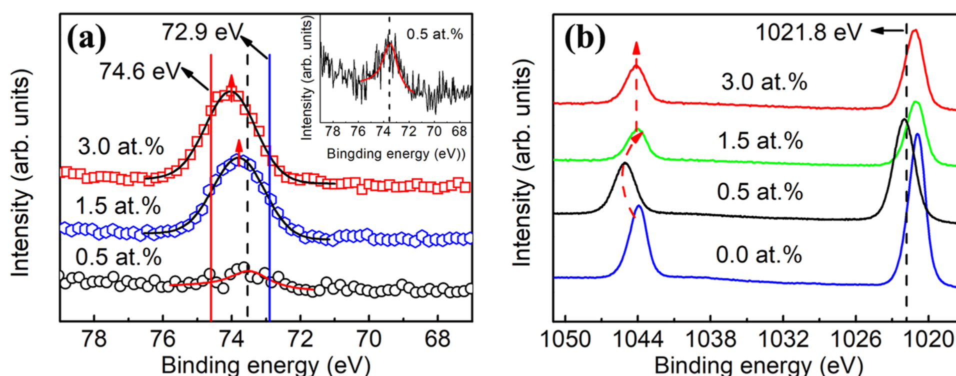

Fig. 6 XPS profiles of Al and Zn in AZO films with different Al doping levels. **a** Al 2*p*, **b** Zn $2p_{1/2}$ and Zn $2p_{3/2}$. The inset in **a** is an enlarged view of the Al signal for the film with an Al doping level of 0.5 at.%

of the conductivity of sol–gel-derived AZO films. Second, some of the soluble Al atoms formed defect complexes, like $n\mathrm{Al}_{Zn}$–V_{Zn}, which passivated donors and decreased the carrier concentration of the AZO films. More effort should be made to increase the solubility of Al in ZnO films and activate Al_{Zn} as a donor in future work.

4 Conclusions

AZO films were prepared by the sol–gel method. The average optical transmittance of the AZO films was about 85% in the visible region and a minimum resistivity of 4.41×10^{-3} Ω cm was obtained. The carrier concentration of AZO increased with Al dopant concentration in the range of 0.5–3.0 at.%, whereas the carrier mobility decreased. The negative effect of Al dopants on the carrier mobility counteracted their positive effect on the carrier concentration and the resistivity of the films remained almost constant at the optimum Al doping level of 0.5 at.%. The doping efficiency of Al in the AZO films decreased with increasing Al doping level. The maximum doping efficiency of ~ 50% was obtained at an Al doping concentration of 0.5 at.%, where Al was thought to totally dissolve in the ZnO film.

The valence state of Al shifted to the more highly oxidized side at higher doping level and strongly influenced the chemical states of Zn and O in the films, leading to changes in the concentrations of Zn interstitials and adsorbed oxygen. The decrease in compressive residual stress in the films with increasing Al doping level indicated the effective doping of Al in the ZnO lattice in the range below 1.5 at.%. The low solubility of 0.5–1.5 at.% Al in ZnO films was confirmed. Consequently, the low doping efficiency above an Al concentration of 1.5 at.% resulted from the segregation of aluminum oxide at the grain boundaries. Below the concentration of 1.5 at.%, the substitutional Al_{Zn} prevailed in the films. The formation of defect complex $n\mathrm{Al}_{Zn}$–V_{Zn} passivated the donors and decreased the doping efficiency.

Acknowledgements This work is financially supported by the National Natural Science of Foundation of China (nos. 51922026, 51571057, 51202256), the Liaoning Provincial Department of Education (JYT19063) and the Fundamental Research Funds for the Central Universities (no. N170204012).

Compliance with ethical standards

Conflict of interest The authors declare that they have no conflict of interest.

References

1. A. Yildiz, S. Uzun, N. Serin, T. Serin, Scripta Mater. **113**, 23 (2016)
2. R.G. Gorden, MRS Bull. **25**, 52 (2000)
3. Y.Q. Chen, X.J. Zheng, X. Feng, Nanotechnology **21**, 055708 (2010)
4. N. Baydogan, O. Karacasu, H. Cimenoglu, J. Sol-Gel Sci. Technol. **61**, 620 (2012)
5. Z.B. Tang, J. Lin, L.S. Wang, J.S. Luo, J.L. Zhao, H.B. Li, Y.J. Wang, X.Y. Liu, Nanotechnology **28**, 365201 (2017)
6. A. Suzuki, T. Matsushita, N. Wada, Y. Sakamoto, M. Okuda, Jpn. J. Appl. Phys. **35**, L56 (1996)
7. H. Hagendorfer, K. Lienau, S. Nishiwaki, C.M. Fella, L. Kranz, A.R. Uhl, D. Jaeger, L. Luo, C. Gretener, S. Buecheler, Y.E. Romanyuk, A.N. Tiwari, Adv. Mater. **26**, 632 (2014)
8. S. Edinger, N. Bansal, M. Bauch, R.A. Wibowo, R. Hamid, G. Trimmel, T. Dimopoulos, J. Mater. Sci. **52**, 9410 (2017)
9. K. Ellmer, A. Bikowski, J. Phys. D: Appl. Phys. **49**, 413002 (2016)
10. M. Ohyama, H. Kozuka, T. Yoko, J. Am. Ceram. Soc. **81**, 1622 (1998)
11. H. Damm, P. Adriaensens, C. Dobbelaere, B. Capon, K. Elen, J. Drijkoningen, B. Conings, J.V. Manca, J. Dhaen, C. Detavernier, P.C.M.M. Magusin, J. Hadermann, A. Hardy, M.K. van Bael, Chem. Mater. **26**, 5839 (2014)
12. M.H. Nateq, R. Ceccato, Materials **12**, 1744 (2019)
13. I. Hamberg, G. Granqvist, J. Appl. Phys. **60**, R123 (1986)
14. E. Burstein, Phys. Rev. **93**, 632 (1954)
15. K.H. Kim, K.C. Park, D.Y. Ma, J. Appl. Phys. **81**, 7764 (1997)
16. M.J. Alam, D.C. Cameron, J. Vac. Sci. Technol. A **19**, 1642 (2001)
17. A. Bikowski, K. Ellmer, J. Appl. Phys. **116**, 143704 (2014)
18. T. Minami, MRS Bull. **25**, 38 (2000)
19. M.H. Yoon, S.H. Lee, H.L. Park, H.K. Kim, M.S. Jang, J. Mater. Sci. Lett. **21**, 1703 (2002)
20. K. Shirouzu, T. Ohkusa, M. Hotta, N. Enomoto, J. Hojo, J. Ceram. Soc. Jpn. **115**, 254 (2007)
21. J.Y. Noh, H. Kim, Y.S. Kim, C.H. Park, J. Appl. Phys. **113**, 153703 (2013)
22. R.B.H. Tahar, N.B.H. Tahar, J. Appl. Phys. **92**, 4498 (2002)
23. E.M. Mkawi, K. Ibrahim, M.K.M. Ali, M.A. Farrukh, A.S. Mohamed, Appl. Nanosci. **5**, 993 (2015)
24. G.M. Nam, M.S. Kwon, Journal of Information Display **10**, 24 (2009)
25. M.U. Shahid, K.M. Deen, A. Ahmad, M.A. Akram, M. Aslam, W. Akhtar, Appl. Nanosci. **6**, 235 (2016)
26. T. Schuler, M.A. Aegerter, Thin Solid Films **351**, 125 (1999)
27. B. Hu, J. Xu, J. Wang, B. Liu, B. Du, Mater. Lett. **232**, 51 (2018)
28. L. Meng, X.G. Yang, H.Y. Chai, Z.R. Lv, T. Yang, Thin Solid Films **672**, 186 (2019)
29. N. Bandaru, E. Panda, J. Alloy. Compd. **789**, 573 (2019)
30. K.D.A. Kumar, V. Ganesh, M. Shkir, S. AlFaify, S. Valanarasu, J. Mater. Sci. Mater. Electron. **29**, 887 (2018)
31. K.D.A. Kumar, S. Valanarasu, A. Kathalingam, V. Ganesh, M. Shkir, S. AlFaify, Appl. Phys. A **123**, 801 (2017)
32. S. Ullah, F. De Matteis, I. Davoli, J. Electron. Mater. **46**, 6609 (2017)
33. S. Peng, Y.K. Tang, L.M. Jin, Y. Wang, L.Y. Ma, F.F. Cao, Surf. Coat. Technol. **310**, 251 (2017)
34. S. Ghosh, J. Chakraborty, Thin Solid Films **605**, 173 (2016)
35. X.Y. Zhao, H.P. Shen, C. Zhou, S.W. Lin, X. Li, X.C. Zhao, X.Y. Deng, J.B. Li, H. Lin, Thin Solid Films **605**, 208 (2016)
36. K. Vernieuwe, J. Feys, D. Cuypers, K. De Buysser, J. Am. Ceram. Soc. **99**, 1353 (2016)
37. F.A. Garcés, N. Budini, R.D. Arce, J.A. Schmidt, Thin Solid Films **574**, 162 (2015)
38. S. Maniv, W.D. Westwood, E. Colombini, J. Vac. Sci. Technol. **20**, 162 (1982)
39. J.G. Lu, Z.Z. Ye, Y.J. Zeng, L.P. Zhu, L. Wang, J. Yuan, B.H. Zhao, Q.L. Liang, J. Appl. Phys. **100**, 073714 (2006)
40. A. Michels, E. Krill, H. Ehrhardt, R. Birringer, D.T. Wu, Acta. Mater. **47**, 2143 (1999)

41. J.T. Thienprasert, S. Rujirawat, W. Klysubun, J.N. Duenow, T.J. Coutts, S.B. Zhang, D.C. Look, S. Limpijumnong, Phys. Rev. Lett. **110**, 055502 (2013)
42. J.E. Stehr, W.M. Chen, B.G. Svensson, I.A. Buyanova, J. Appl. Phys. **119**, 105702 (2016)
43. M.W. Zhu, H. Huang, J. Gong, C. Sun, X. Jiang, J. Appl. Phys. **102**, 043106 (2007)
44. C.D. Wagner, W.M. Riggs, L.E. Davis, J.F. Moulder, *Handbook of X-ray photoelectron spectroscopy*, 1st edn. (Perkin Elmer Corporation, Eden Prairie, 1979), pp. 54–55
45. A. Momot, M.N. Amini, G. Reekmans, D. Lamoen, B. Partoens, D.R. Slocombe, K. Elen, P. Adriaensens, A. Hardy, M.K. Van Bael, Phys. Chem. Chem. Phys. **19**, 27866 (2017)
46. S.B. Zhang, S.-H. Wei, A. Zunger, Phys. Rev. B **63**, 075205 (2001)
47. P. Erhart, K. Albe, A. Klein, Phys. Rev. B **73**, 205203 (2006)
48. F.F. Cao, C.P. Li, M.J. Li, H.J. Li, X. Huang, B.H. Yang, Appl. Surf. Sci. **447**, 173 (2018)
49. M. Chen, X. Wang, Y.H. Yu, Z.L. Pei, X.D. Bai, C. Sun, R.F. Huang, L.S. Wen, Appl. Surf. Sci. **158**, 134 (2000)
50. C. Singh, E. Panda, RSC Adv. **6**, 48910 (2016)
51. S.R. Dhage, A.C. Badgujar, J. Alloy. Compd. **763**, 504 (2018)
52. H. Aguraa, A. Suzukia, T. Matsushitaa, T. Aokia, M. Okudab, Thin Solid Films **445**, 263 (2003)
53. S.Y. Myong, S.J. Baik, C.H. Lee, W.Y. Cho, K.S. Lim, Jpn. J. Appl. Phys. **36**, L1078 (1987)
54. F. Khan, S.H. Baek, J.H. Kim, J. Alloy. Compd. **709**, 819 (2017)
55. V. Anand, A. Sakthivelu, K.D.A. Kumar, S. Valanarasu, V. Ganesh, M. Shkir, S. AlFaify, H. Algarni, J. Sol Gel Sci. Technol. **86**, 293 (2018)
56. K. Lin, Y.Y. Chen, K.Y. Chou, J. Sol-Gel Sci. Technol. **49**, 238 (2009)

Publisher's Note Springer Nature remains neutral with regard to jurisdictional claims in published maps and institutional affiliations.